Low Aspect Ratio High-Lift Wing Design for Automotive Racing Applications

Sajana S. Ratnayake[1] *and* Timothy T. Takahashi[2]
Arizona State University, Tempe, AZ, 85281, USA

This paper focuses on the design of front wings for Formula 1 cars focusing on how to keep flow attached over the wing while maximizing downforce at low speeds and cornering. We explore Single and Multi-element front wings to understand the nature of airflow over low aspect ratio wings along with techniques used to improve downforce while preventing or limiting flow separation. In addition, race car wings with multiple elements are also considered and evaluated to see the differences they make in downforce generation.

Nomenclature

MACH = Mach number
ALPHA = Angle of attack
S = Spanwise index of vortex element
C = Chordwise index of vortex element
X = X coordinate
Y = Y coordinate
Z = Z coordinate
C = Local chord length
X/C = Percent location of point on the chord
DCP = Local pressure coefficient
CNC = Sectional normal force coefficient multiplied by local chord
CN = Sectional normal force coefficient
CP = Control point
C_p^* = Critical Pressure Value
M_{cr} = Critical Mach Numbers
CFD = Computational Fluid Dynamics

I. Introduction

Over the past fifty years, aerodynamic design of racing cars has changed significantly as aviation concepts have been embraced to improve the aerodynamic performance of racing cars. This paper focuses our research considering the reasons behind some of the changes and improvements we have seen on recent Formula 1 cars. We will use a mixture of potential flow analysis and volume-grid CFD to understand the rationale for changes enthusiasts have seen in recent years. Here we concentrate on features seen in the evolution of front wing geometry. We discuss the potential developments that will take place in the upcoming years.

II.Evolution of Front Wing Geometry

To begin, let us consider the evolution of the wing geometry of the front down-force generating wing of Ferrari Formula 1 cars over the past fifty years; see FIGURE 1 (overleaf). Beginning with FIGURE 1a, consider the 1971-72 season Ferrari 312-B2 with a simple mildly cambered single-element front wing with small endplates. [1] There is no visible change in airfoil incidence, thickness, or camber across its span. Next consider FIGUREs 1b and 1c, the very competitive Ferrari 312T of 1975-1980. [2] Both the Niki Lauda and Gilles Villeneuve driven cars have a highly aft-cambered, single element front wing with small

[1] MS Student – Mechanical Engineering, School for the Engineering of Matter, Transport, and Energy, Arizona State University, Tempe, AZ, 85287. AIAA Student Member.
[2] Professor of Practice, Aerospace and Mechanical Engineering, School for Engineering of Matter, Transport & Energy, P.O. Box 876106, Tempe, AZ, 85281, Associate Fellow AIAA

endplates; the Villeneuve car (a 312T5 from the 1980 season) appears to have considerably more camber as well as visible span-wise variation in camber compared to the earlier Lauda car. [3]

a 

b 

c 

FIGURE 1 – Front Wings as found on Ferrari F1 Cars from the 1970s.

The state of the art does not appear to have substantially changed throughout the 1980s or early 1990s. The 1987 Ferrari F1-87 has a two-element front wing, but retains uniform airfoil sections, gap, overlap and incidence across its span; see FIGURE 2a. [4] Moving into the 1990s with the Ferrari 642, we continue to see the application of simple two-element wings with modest endplates; see FIGURE 2b. [5] It isn't until 1992 with the Ferrari F92A that we see a front wing with an unusual planform; and then the complexity is found on the trailing edge of the second element; see FIGURE 2c. [6] Careful inspection of FIGURE 2c shows that the gap and overlap between the front and second element is essentially uniform across its span; neither is there evident spanwise camber or incidence variation on the front element. Only with the Ferrari F412T1 of 1994 do we begin to see front wings with clear spanwise "twist;" see FIGURE 2d. [7]

a b c d

FIGURE 2 – Ferrari Formula 1 cars of the 1980's and 1990s.

At Ferrari the design paradigm began to change rapidly in the early 2000's. Compare FIGURE 3a with 3b, the F2003-GA to the F2005. We see that the F2003-GA has two-element wing, some spanwise variation on the front wing… moderate camber, but large spanwise planform variation on the second element. [8] The F2005 has a highly three-dimensional aerodynamic surface with three-elements along the vehicle centerline, and two elements outboards. [9]

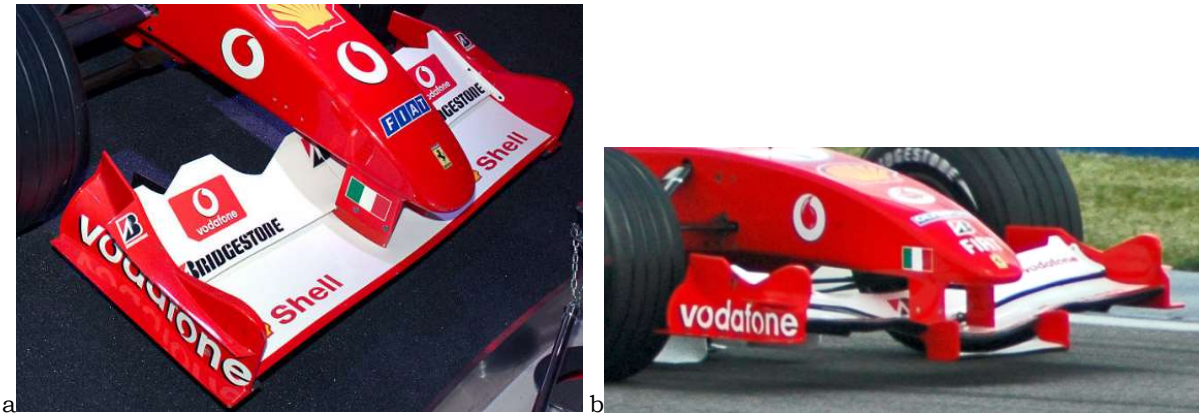

a b

FIGURE 3 – F2003-GA vs F2005.

The ban of ground effects in 1983, due to car crashes because of porpoising, left the teams developing discrete front and rear wings in association with much simpler body panels to generate downforce. This led to the top teams with the most budget developing even more advanced front wings. Consider the 2015 SF15-T wings designed by Ferrari. Notice the complex shapes utilized in 2015 as seen in FIGURE 4 where not only are there multiple horizontal wing elements but also vertical fins, and U-shaped undercuts that help obtain better pressure distributions on both upper and lower surfaces of the front wing. [10]

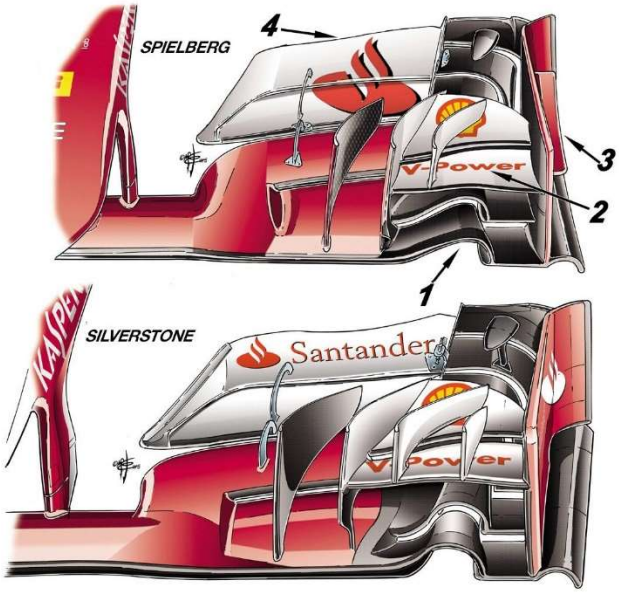

FIGURE 4: SF15-T Ferrari Front Wing in 2015

This, however, led to an unfair advantage to the top teams in Formula 1 as teams with less budget were left far behind and the top teams were able to develop more complex front wing designs due to their availability to fund additional CFD and wind tunnel test time.

This began the start of the FIA budget caps; stricter rules restricted the design of front wings. [11] As a result, the front wings became simpler and by 2021, the number of elements were restricted to only 5 along with additional restrictions on camber and twist. [12] This led to a more even spread of the grid and reduced the advantage that top teams had over the less funded teams.

FIGURE 5: Ferrari Front Wing in 2021 Season

In 2022, the new generation F1 car was released and latest update from the FIA limits front wings to only 4 elements and provides limited planform modifications and twist restrictions in order to bring the grid even closer to one another to encourage closer racing. [13] Along with this update, comes the re-introduction to ground effect being legal after the ban was implemented in the 1980s. While this means that lesser work needs to be done by the front wing, it now requires teams to do further research to redirect flow from the front wing to aerodynamic and cooling elements more strategically to utilize the ground effect more effectively. This proved to be a challenge in the early 2022 season; many teams fielded cars suffering from porpoising as a result of the lower surface of the car bottoming out. This led to quick evolutions of the front wing and height adjustments to improve airflow under the car. [14]

FIGURE 6 - Current Front Wing Designs at Start of Formula 1 2022 Season:
a) Aston Martin, b) McLaren, c) Alpha Tauri, d) Ferrari

All of these, and many more additions, led to an improved wing design capable of increasing downforce (negative lift) while reducing drag forces that are acting upon the front wing. The downforce applied to a wing is also important to keep the car under control as an unbalanced load on the front and rear wheels of the car can lead to spinouts or locking up of wheels which are detrimental to a race as every fraction of a second counts for a good race result.

Having some experience designing wings for aircraft, we became curious as to the motivation for these design changes. This work begins with first principles then moves on to potential flow models attempting to answer several questions.

First, is the move from highly cambered single to multi-element airfoils well justified?

Second, is the move from simple quasi-2D wings (extruded airfoils with endplates) to complex planforms and twist geometries well justified?

Our research explores the evolution of the front wing, starting from very basic wings to adding multiple elements and understanding how the new wing shapes are more beneficial to prior wings in previous seasons.

III. Aerodynamic Flow Basics

Before we dive deeper into the analysis of front wing evolution and its performances, we must first understand some general insights we can gather from aerodynamics and flow conditions.

A. Flow Conditions

Formula 1 cars can have speeds upwards of 200 mph (Mach 0.26) when traveling down long straights in a track but can be travelling as slow as 50 mph (Mach 0.065) in some corners. This reflects unit Reynolds numbers from ~500,000 to 1.8 million per foot. Given typical wing element chords of 4 to 8-inches (0.33 to 0.66-ft), this means that we can expect to see various wing elements working at Reynolds numbers, $Re = \frac{\rho u L}{\mu}$, in the ~100,000 to ~500,000 range. Similarly, the dynamic pressure, $q = \frac{\rho u^2}{2}$, is likely to range from 5-lbf/ft^2 in the tightest of corners to ~100-lbf/ft^2 at the end of a long straightaway.

B. Limits of Lift and Pressure

AMO Smith [15] notes that the theoretical upper limit of lift in a potential flow field is for an airfoil that has a circular camber. This creates the possibility of the 2 stagnation points to be at the same point by forcing the rear and front stagnation points to occur at the same point; see FIGURE 7. This is of course unrealistic and is only a theoretical maximum as this assumes completely inviscid flow and an extremely high amount of circulation taking place. If this case were possible, it would be able to obtain a maximum lift coefficient, C_l, of 4π or ~12.57.

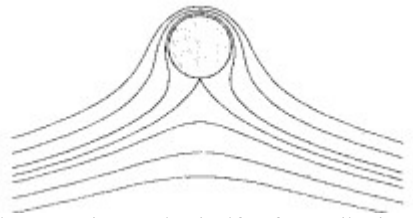

FIGURE 7 – Maximum Theoretical Lift of a Cylinder with Circulation

However, this is of course not the reality and we will have to calculate the maximum lift coefficient based on the lift equation: $C_L = \frac{2L}{\rho u^2 Sref}$ where $C_L = lift\ coefficient$, $L = Lift\ (or\ in\ our\ case, downforce)$, $\rho = density\ of\ air$ and $S = planform\ reference\ \ area.$

Current Formula 1 front wings have widths of approximately 6.5 ft and chord lengths of approximately 1 ft: thus, a rough planform with *Sref* ~ 7-ft^2 reference area. The operating lift coefficient depends upon the downforce required, the speed and the wing planform reference area.

The maximum $C_L$is expected to be around 1.75 – 2.5 based on sources available online [16]. For our design, we will start will a target C_L of 2 and seeing if this is an achievable target and increase our goal once we are happy with a solution obtained.

The highest positive pressures that can act upon the wing surface is governed by stagnation; where $C_p = \frac{p-p_\infty}{q_\infty} = +1$. Note $C_p = pressure\ coefficient$, $p = static\ pressure\ at\ given\ point$ $p_\infty = freestream\ static\ pressure$ and $q_\infty = freestream\ dynamic\ pressure$. We want stagnation to be localized at a single point somewhere near the wing leading edge, elsewhere on the wing *Cp* < +1 where the local flow is moving aft at some reasonable airspeed.

Both windward and leeward side pressures are limited to the 70% vacuum limit that Mayer [17] suggests as a practical limit. This gives us the lower C_p limit at: $C_p^* = \frac{p-p_\infty}{0.7 p_\infty M_\infty^2}$. Which, under isentropic conditions, can be written as: $C_p^* = \frac{1}{0.7M_\infty^2}\left[\left(\frac{1+0.2M_\infty^2}{1+0.2M^2}\right)^{3.5} - 1\right]$.

An alternative method that can be used for calculating C_p^* is Küchemann's critical pressure equation: [18]

$$C_p^* = \frac{2}{\gamma M_\infty^2}\left\{\left(\frac{2}{\gamma+1}\right)^{\frac{\gamma}{\gamma-1}}\left(1+\frac{\gamma-1}{2}M_\infty^2(cos\phi)^2\right)^{\frac{\gamma}{\gamma-1}}-1\right\}$$

For an unswept wing, this equation becomes:

$$C_p^* = \frac{2}{\gamma M_\infty^2}\left\{\left(\frac{2}{\gamma+1}\right)^{\frac{\gamma}{\gamma-1}}\left(1+\frac{\gamma-1}{2}M_\infty^2\right)^{\frac{\gamma}{\gamma-1}}-1\right\}$$

FIGURE 8, demonstrates the practical and physical limits of leeward side suction. At 200-mph (Mach 0.26), a 70% vacuum places an upper limit to suction at *Cp* ~ -14.8 whereas the *Cp** sonic limit places a practical limit so that *Cp* > ~ -9.4 to ensure shock-free subcritical flow.

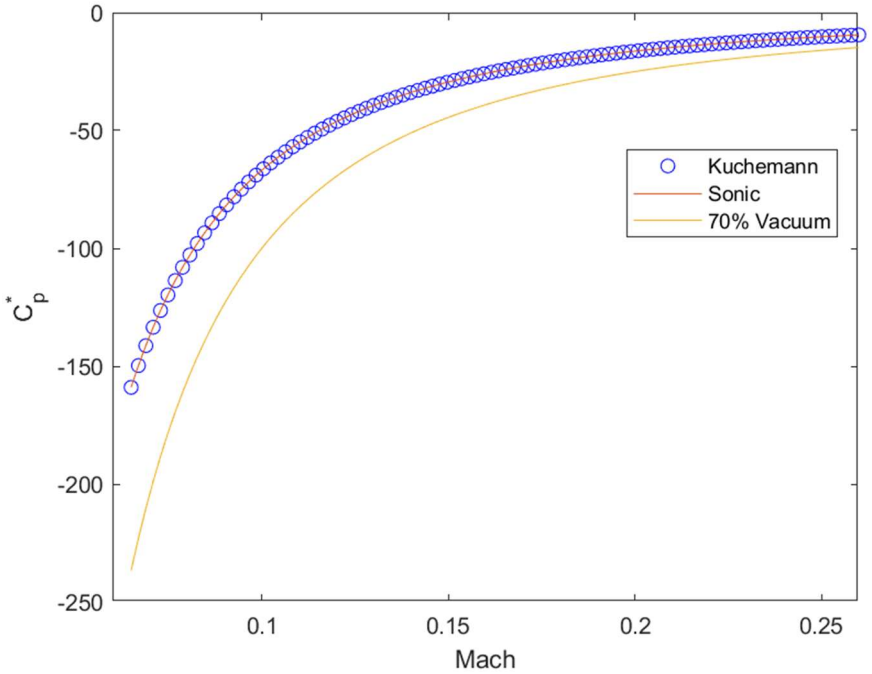

FIGURE 8 – Limiting Pressures as a function of Road Speed

As Formula 1 wings are still relatively lower aspect ratio compared to airplane wings, we need to increase the amount of downforce as much as possible while ensuring that flow separation is prevented. In order to do this, we will utilize a Stratford separation limit when calculating C_p^* like when A. M. O. Smith conducted his research. [15] The main reason why Stratford's method for predicting flow separation is utilized for this research is because our flow is mostly turbulent, and we want to ensure that we minimize or prevent flow separation along the wing.

Stratford's equation for predicting flow separation [19] (which is a pessimistic or "conservative" approach, in that it predicts separation somewhat earlier than test data) can be written as: $\frac{\overline{C_p}\,[x\left(\frac{d\overline{C_p}}{dx}\right)^{\frac{1}{2}}}{(10^{-6}R)^{1/10}} = S$ where S is 0.39 for $\frac{d^2p}{dx^2} \geq 0$ or 0.35 for $\frac{d^2p}{dx^2} \leq 0$.

$\overline{C_p}$ is related to C_p as shown by the equation below:

$$C_p(x) = 1 - \frac{1 - C_{p,T.E.}}{1 - \bar{C}_{p,sep}}[1 - \bar{C}_p(x)]$$

Where $C_p = 1 - \left(\frac{u_e}{u_\infty}\right)^2$, $C_{p,T.E.} = 1 - \left(\frac{u_e}{u_\infty}\right)_{T.E.}^2$ and $\overline{C_p} = 1 - \left(\frac{u_e}{u_0}\right)^2$

For this work, we will take S as 0.39 and show that:

$$\overline{C_p} = 0.645\left\{0.435R_0^{\frac{1}{5}}\left[\left(\frac{x}{x_0}\right)^{\frac{1}{5}} - 1\right]\right\}^{2/n}$$

When $\overline{C_p} \leq \frac{(n-2)}{(n+1)}$

And,

$$\overline{C_p} = 1 - \frac{a}{\left[\left(\frac{x}{x_0}\right) + b\right]^{1/2}}$$

When $\overline{C_p} \geq \frac{(n-2)}{(n+1)}$ where a and b are arbitrary constants based on where $\overline{C_p} = \frac{(n-2)}{(n+1)}$

Stratford finds that n ≈ 6, which gives us the following equations:

$$\overline{C_p} = 0.645\left\{0.435R_0^{\frac{1}{5}}\left[\left(\frac{x}{x_0}\right)^{\frac{1}{5}} - 1\right]\right\}^{1/3}$$

When $\overline{C_p} \leq \frac{4}{7}$

And,

$$\overline{C_p} = 1 - \frac{a}{\left[\left(\frac{x}{x_0}\right) + b\right]^{1/2}}$$

When $\overline{C_p} \geq \frac{4}{7}$ where a and b are arbitrary constants based on where $\overline{C_p} = \frac{4}{7}$

The problem with highly twisted and highly cambered wings is that as we increase the camber and incidence of the wing, the airfoil starts to generate more drag and decreases the benefits due to downforce. So, as we go to higher angles of incidence, a larger component of the wing will be creating drag rather than downforce, as we see in FIGURE 9 using a S1210 airfoil for demonstration and choosing an arbitrary point on the airfoil which initially only creates downforce at the given chord location.

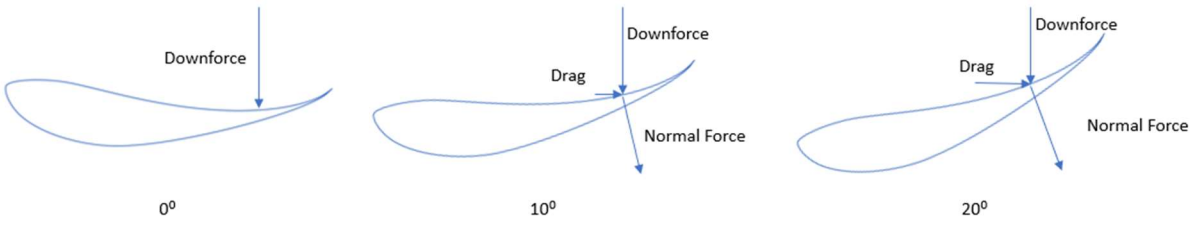

FIGURE 9: Drag Increases and Downforce Decreases as Incidence Increases

Similarly, if the camber profile of a wing is increased by a large amount, the drag component of the wing also amplifies since the angle of the contour increases. This can be seen in FIGURE 10 as we increase the percent camber of the S1210 airfoil to 100%, 150% and 200% for a fixed chord length.

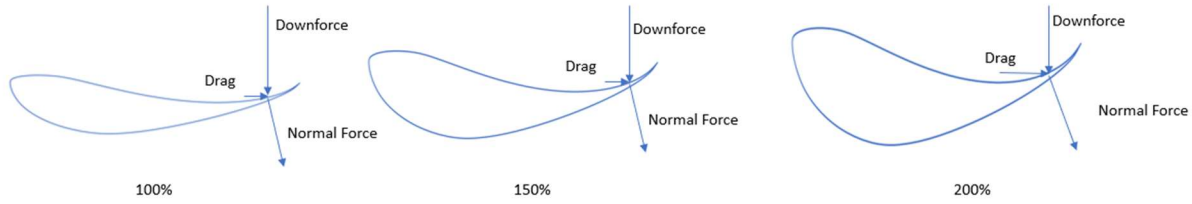

FIGURE 10: Drag Increases and Downforce Decreases as Local Surface inclination (because of camber profile being increased)

Because of these highly cambered and highly twisted designs, we need to be aware when we are designing the wing as there comes a point where the normal force acting on the wing because of increased pressure, creates more drag than downforce.

In order to make sure that the flow remains attached, we need to ensure that the pressure distribution over the wing is smooth and uniform with no sudden pressure drops or rises to trigger the Stratford separation criteria.

Our first step in starting our wing design is calculating the limits for when separation will occur on our wing based on Stratford Criterion. The initial attempt was to achieve a target pressure distribution using Stratford as discussed in the current section of this paper. However, obtaining the required pressure distribution seemed impossible to solve analytically. Therefore, Küchemann's critical pressure equation was used first to ensure that the wing was subcritical (i.e., shock free) and then the inviscid pressure profiles were evaluated using the Stratford criteria to ensure that flow separation does not occur. Using Küchemann's critical pressure equation, a minimum pressure of -10.4 was obtained for a 35° swept wing.

IV. Some Issues Seen in Recent Automotive Wing Design Papers

In work done recently by Castro & Rana [20], we see them exploring multiple aspects of Formula 1 wing design including the structure, material, weight, and aerodynamics. They explored the changes made in aerodynamics due to the addition of endplates to a Formula 1 wing and the aerodynamic pressures on an optimized wing designed by the authors. We can see here (reference FIGUREs 11 and 12) that their wings exhibit peak suction quite far forwards, as we suggested following Stratford (recall FIGURE 8). However, the wings shown in FIGUREs 12 and 13 exhibit strong spanwise variation in pressure fields even with large endplates fitted. Pressures shown in this paper are absolute, rather than in coefficient form, but if we assume that stagnation pressure is ~+5,500 Pa, then FIGURE 12 exhibits peak suctions with Cp~-3.6 and FIGURE 13 exhibits peak suctions with Cp~-5.8. While the suction peak is somewhat "softer" than the Stratford limiting pressure distribution, the contours on the inboard portion of the wing shown in FIGURE 13 seems reasonably aligned with a Stratford-style pressure recovery profile from a peak suction around 30% chord.

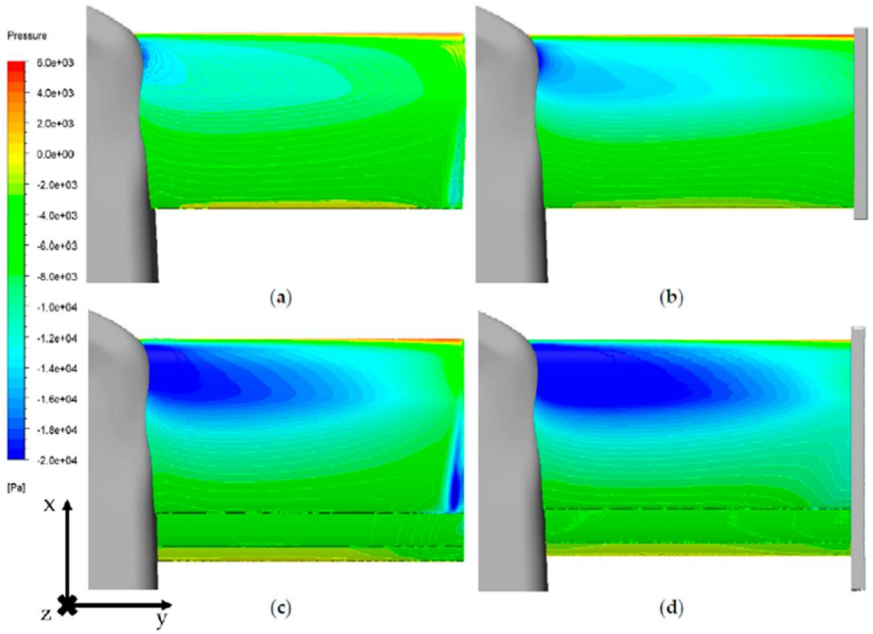

FIGURE 11: Castro & Rana Demonstrating the Effect of Endplates on Single and 3 Element Wings

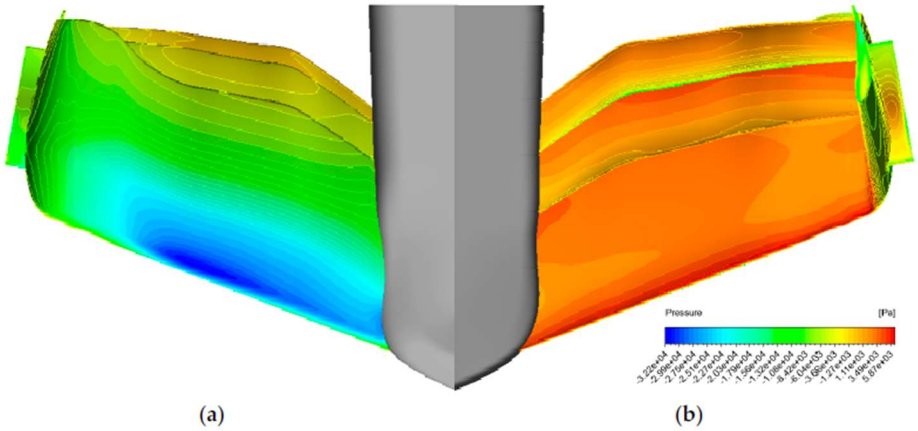

FIGURE 12: Castro & Rana Plotting the Pressure Distribution of their Optimized Wing Design

As we see from FIGURES 2 and 3, Formula 1 wings have had somewhat higher aspect ratios in the past. This has the upside of causing less drag, however, has the problems of increased flow separation and lesser surface area for increasing downforce. Earlier wings also tend to have an unswept leading edge which (we realize) also increases flow separation at the leading edge. In the new era of Formula 1 wings, we see the FIA and teams move away from these issues by having a lower aspect ratio overall compared to previous years and also a swept leading edge which helps attach the flow better as we will see in our research as well.

V. Motivation for Current Research

The previous work mentioned in Section IV left us curious about how much more improvement can be done on the Formula 1 wings simply by understanding the airflow over highly twisted, low chord length wings in order to optimize airflow resulting in high downforce and less drag.

We were also curious to see how much we can utilize a Vortex Lattice solver algorithm (such as VORLAX) to conduct the initial understanding of airflow over the wings to reduce time spent on a finite volume method (such as ANSYS Fluent). As a result, we can generate camber and thickness profiles on VORLAX to understand airflow in a shorter amount of time and then transfer our knowledge to ANSYS Fluent as we will have a better understanding of the airflow to tweak the wing to be optimal with fewer iterations.

In addition, this also gave us the opportunity to explore where Formula 1 front wings might go in the future to improve performance even further while ensuring safety as well. Section VII discusses our predictions along with reasoning to explore what changes might happen in the upcoming years to develop said wings.

VI. Findings Through Current Research

Our current research defines a method that is capable of designing multi-element wing designs for race car applications. We synthesize single element wings and multi-element wings. We propose some alternate shapes and make some recommendations based upon our observations.

A. Single Element Front Wing

The synthesis of a single element wing was relatively straightforward based on our experience designing aircraft wings. The quickest way to do this was to perturb each control point (in our case 4 control points were utilized) with varying angles of incidence and camber. To make the synthesis faster, we used a single camber profile with thickness. The camber profile was the S1210 which was also utilized by Castro and Rana in their research for recent automotive wing design studies. FIGURE 13 below shows the control points used for the single element wing where control point 1 is the centerline of the wing, control point 2 and 3 are the middle regions of the wing and control point 4 was the tip of the wing.

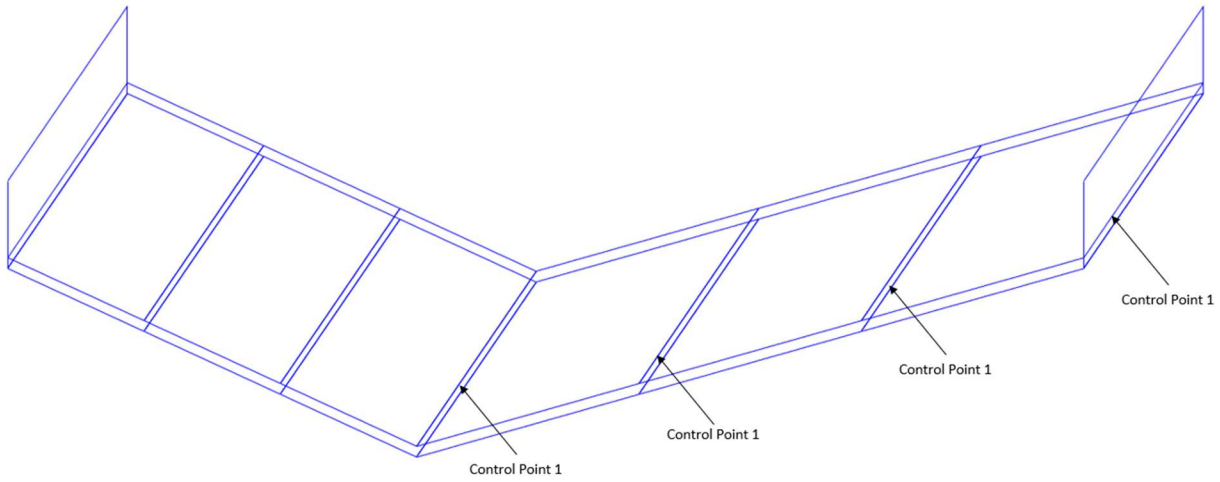

FIGURE 13: Control Points Utilized for Single Element Wing

Similar to wing design research conducted by Ratnayake & Takahashi in earlier publications, the control points were perturbed at each control point to obtain the predicted behaviors of the airflow which can then be superimposed to obtain a necessary lift distribution. [21][22] FIGURE 14 shows the lift characteristics obtained when using angles of incidence of 5.71° (which is equivalent to arctan(0.1) and 100% S1210 profiles.

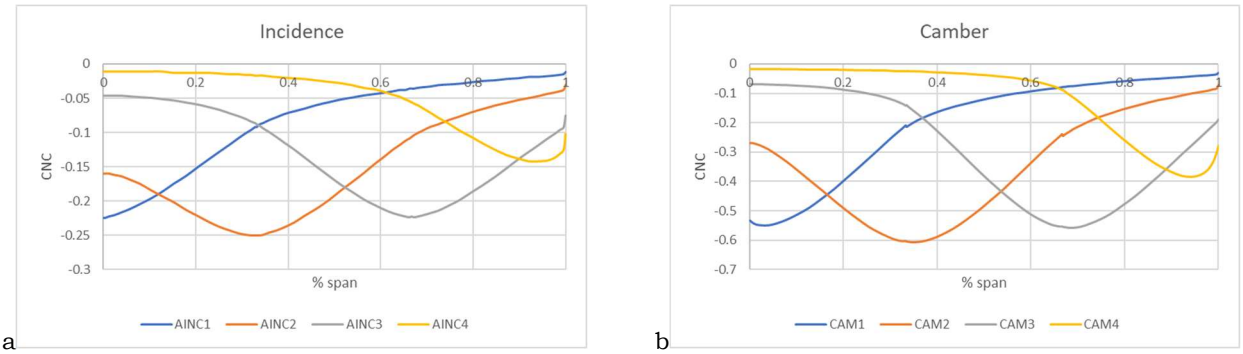

a b

FIGURE 14: Perturbed a) Angle of Incidence and b) Camber

Additionally, overall angle of attack of the wing was also perturbed at 1° to use as a possible perturbation to solve for the required target lift.

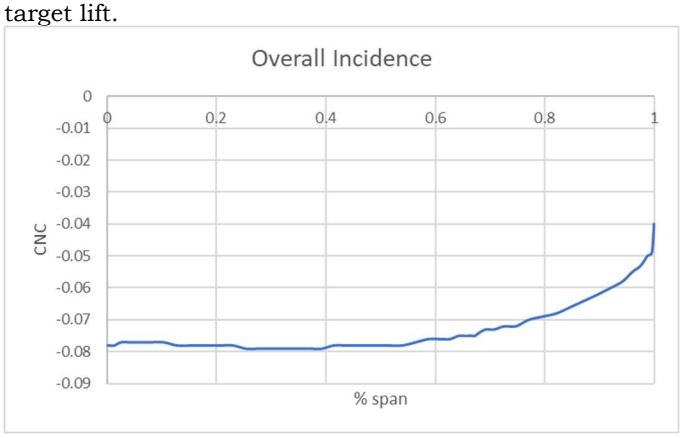

FIGURE 15: Overall Angle of Wing

Using this information, a solver was created to obtain a target lift distribution while maintaining flow attachment. The target was reached using the following equation.

$$R^2 = 100 * \left(\frac{(Lift - Ideal\ Lift)}{Ideal} Lift\right)^2 + \left(\left(\frac{(0.8 * Critical\ Pressure) - Pressure}{0.8 * Critical\ Pressure}\right)^2\right) + \left(\frac{Min\ Pressure\ Location - 0.15}{0.15}\right)^2$$

In the above equation, the multiplier in front of the lift terms can be adjusted to bias the amount by which to prefer solving the ideal lift curve as opposed to achieving the pressures and pressure locations. For instance, in the 6-panel method, this number was set to 10,000 to bias the solving of the ideal lift curve for better results. This of course means that the min pressure needs to be monitored manually as well to ensure no separation occurs throughout the wing.

We see in FIGURE 16 that the initial solution did not meet the expected lift curve exactly when simulated again on VORLAX. The presence of the endplate prevents the wings from being able to completely shed all lift before reaching the planform limit. The “calculated spanwise lift curve” and “actual spanwise lift curve” deviate slightly because of the substantial twist and camber of the synthesized configuration; while linear superposition of the potential function holds – the direction sines and cosines that pressures act upon cannot be simplified as cos(θ)==1, sin(θ)==0 as is common with “classical” thin airfoil theory.

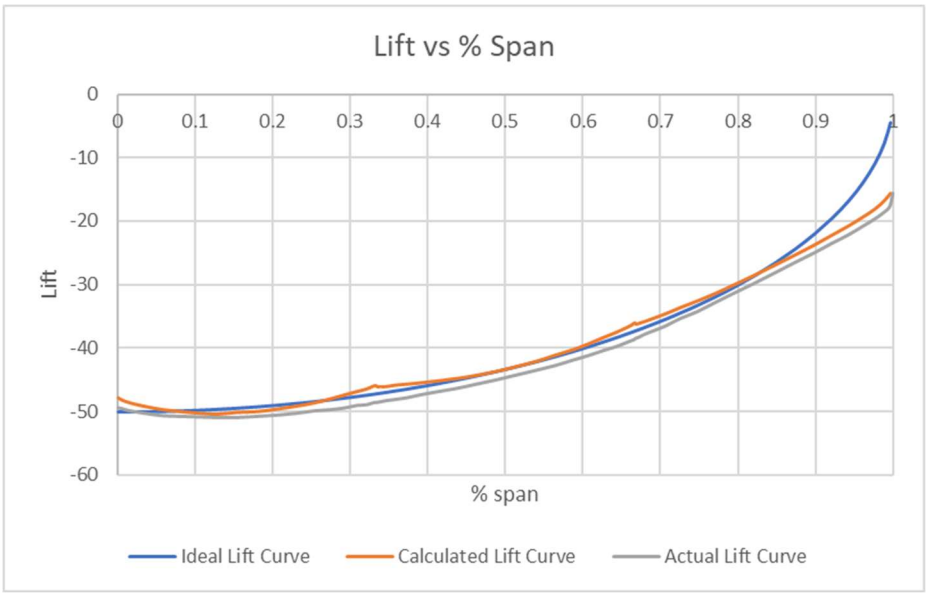

FIGURE 16: Single Element Lift Distribution

The upper and lower surface pressure distributions obtained from this generated wing design can be seen in FIGURE 17 below. We can see that this wing lifts "down" as the lower surface pressures are more negative than the upper surface pressures; this is consistent with the design point.

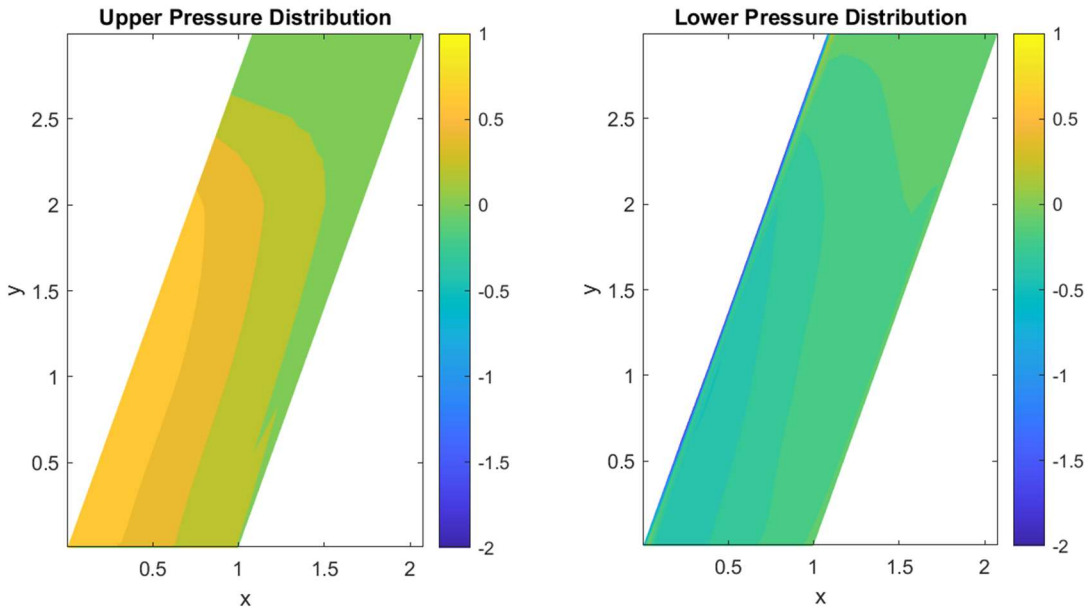

FIGURE 17: Single Element Pressure Distribution

This gave the following parameters for the single element front wing. We see that an elliptically loaded single element wing has both "wash out" and a reduction in camber from centerline to tip.

TABLE 1: Parameters for a Single Element Wing

Control Point	Camber	Angle of Incidence in Degrees
1	50%	-1.72
2	40%	-1.15
3	30%	-1.15
4	20%	1.72

It's important to note here that camber and angle of incidence are both acting to create downforce. So, the camber is aligned with the concave side facing up and the convex side facing down such that a downward lift is generated. Similarly, the angle of incidence is negative here such that downforce is being generated instead of upward lift.

B. Single Element Design in a Multi Element Panel

Initially, we attempted to synthesize multiple elements of the wing in a single-step process. We found that worked poorly as there were instances when the front element was highly twisted, only for the rear element to be highly twisted in the opposite direction, which eventually leads to no net work done by both elements of the wing. This happens because the solver looks for a solution where the ideal lift curve can be achieved. However, by doing so, the solver tries to twist the front and rear elements in opposite directions to reach the target lift distribution.

This led us to the idea of first solving the parameters needed for the frontmost wing element, and then solving for the elements that follow behind it. However, this meant that a different lift distribution must be set as the target for each case that is run. For instance, if the max lift needed at the centerline was 40, we can choose the first wing element to have 20 as the max. Again, it is not absolutely necessary to distribute the lift generation equally among multiple elements of the wing.

Using this method, we obtained the following lift and pressure distributions for a single element of a multi-element wing.

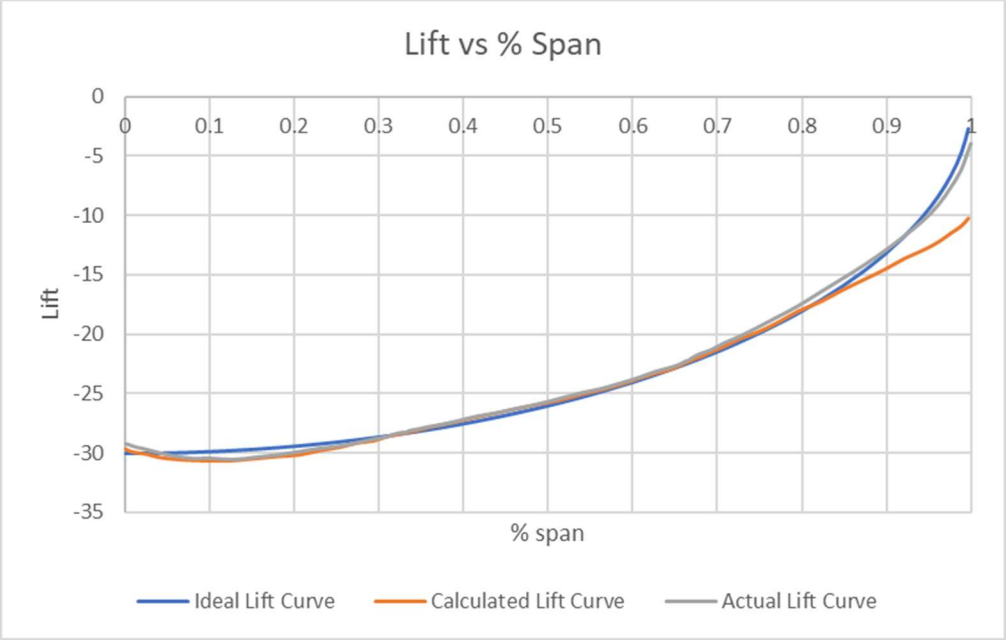

FIGURE 18: Lift Distribution for a Single Element of a Multi Element Front Wing

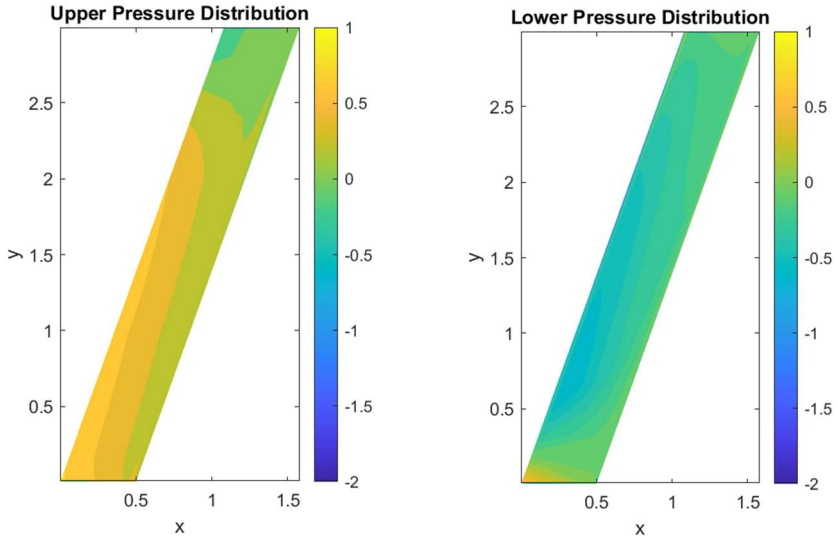

FIGURE 19: Pressure Distribution for a Single Element of a Multi Element Front Wing

We see here that the lift curve and pressure distribution obtained for the front element being well resolved such that the lift curve is close to the ideal lift curve and the pressure distributions are smooth and there is no lumpiness going on.

The parameters obtained for this portion can be seen in TABLE 2.

TABLE 2: Parameters for Single Element of a Multi Element Wing

Control Point	Camber	Front Angle of Incidence in Degrees
1	50%	-2.29
2	40%	-1.15
3	30%	-1.15
4	20%	1.15

Recall here that both camber and twist are acting such that downforce is generated as a result. Overall, the geometry will have a concave panel upwards, convex panel downwards and a nose down geometry.

C. Multi Element Design in Multi Element Panels

When designing a high downforce wing, the angles of incidence tend to be very high (some cases that were run had angles of incidence going up to 45º). This leads to the rear element of the wing being highly dependent on the front element of the wing. Initial cases run for this scenario had fixed planforms of the wing where only camber and twist were altered. What became quickly apparent was that as the angle of incidence increased, the elements leeward of the airflow get blocked by the windward elements. As a result, the leeward elements need to be modified each time a wing was synthesized. The modification conducted was that the leeward wing element would always start just above the position where the windward element ends, however moved up in the z-axis by 0.1 feet (this value was arbitrary to ensure that there was some distance between the elements). Using this modification helped ensure that the elements behind the leading element of the wing had sufficient airflow to generate downforce and not lead to flow separation.

Another issue that was encountered was that sometimes, the solver utilized would have highly cambered wingtips. This sometimes led to unusual thicknesses as the central regions of the wing might be narrower than the outward regions of the wing. This is of course not realistic as it is preferred to have t/c reducing as one moves away from the center point of the wing. By having the thickness decrease as the wing moves

outward, the structures required to support the wing can be achieved more realistically as the support structures can then reduce in thickness over the span of the wing. This problem was overcome by having the camber fixed at each control point. For the cases run in this research, 50% camber was used at control point 1 (center line), 40% at control point 2, 30% at control point 3 and 20% at control point 4 (wingtip). This ensured that camber was reducing as we went from the center of the wing to the wing tip.

This then made so that the solver only needs to find the incidence at each control point to obtain the target lift and pressure distributions which were somewhat more straightforward to complete. However, there were instances where the solver algorithm would get lost and not generate lift and pressures that were expected to be seen.

FIGURE 20 shows the control points that already have parameters solved for in step 1 and the control points that will be solved in the second iteration.

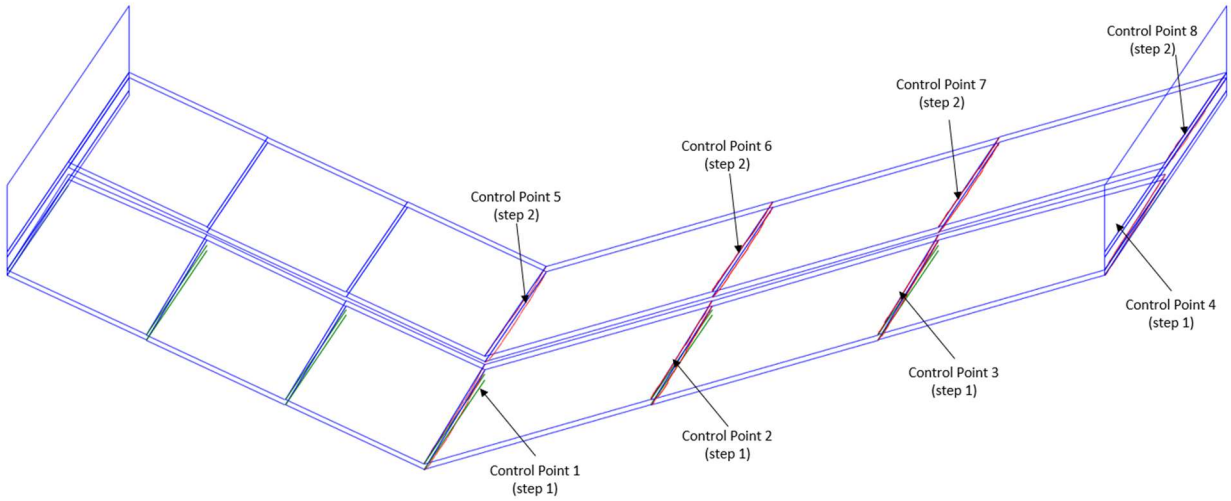

FIGURE 20: Control Points for 2-step Method

Instead, a different approach was taken to solve the second element twist configurations. Using the Excel solver that was created for the previous element synthesis, the twist configurations were changed manually as needed to achieve the required lift and pressure distributions. This allowed the user to change the twist quantities by reasonable amounts and more intuitively make changes to obtain the required targets. Could an alternate approach have been taken to automate this process? Possibly, yes. However, it was relatively straightforward to achieve the target manually than automating a new solver.

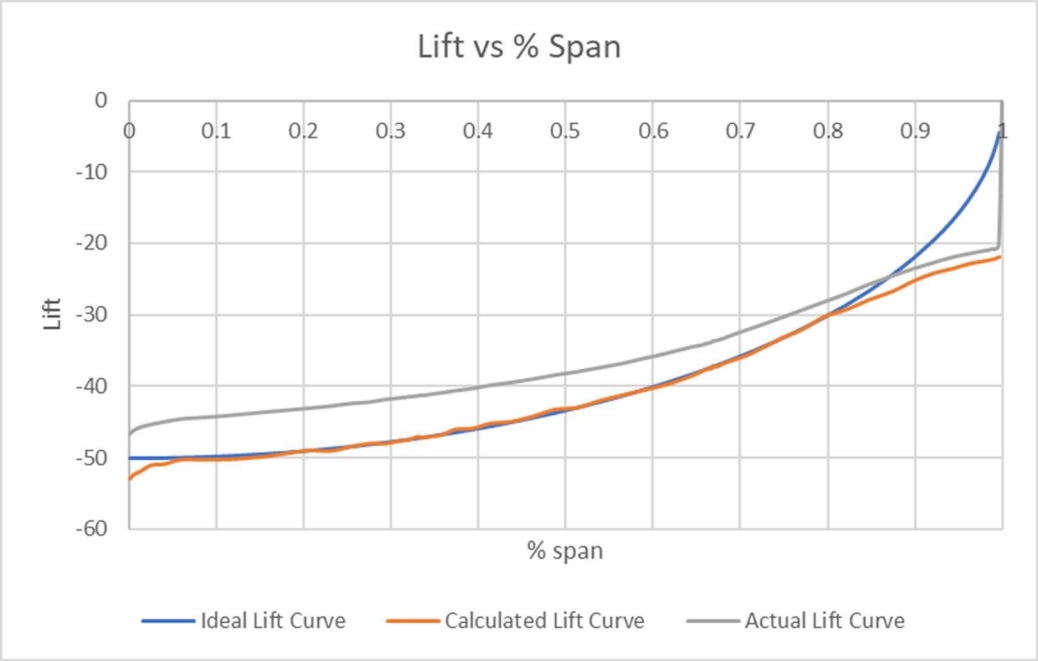

FIGURE 21: Lift Distribution for a 2 Element Wing

We see here that the calculated lift curve and simulated lift curve do not match in this case. This is because as we're getting into such high angles of attack (see TABLE 3), the direction sines and cosines that pressures act upon cannot be simplified as cos(θ)==1, sin(θ)==0 as is common with "classical" thin airfoil theory. This is especially because the geometry changes due to the large angles that are being perturbed (see FIGURE 9).

FIGURE 22 shows the pressure distribution achieved from this synthesis.

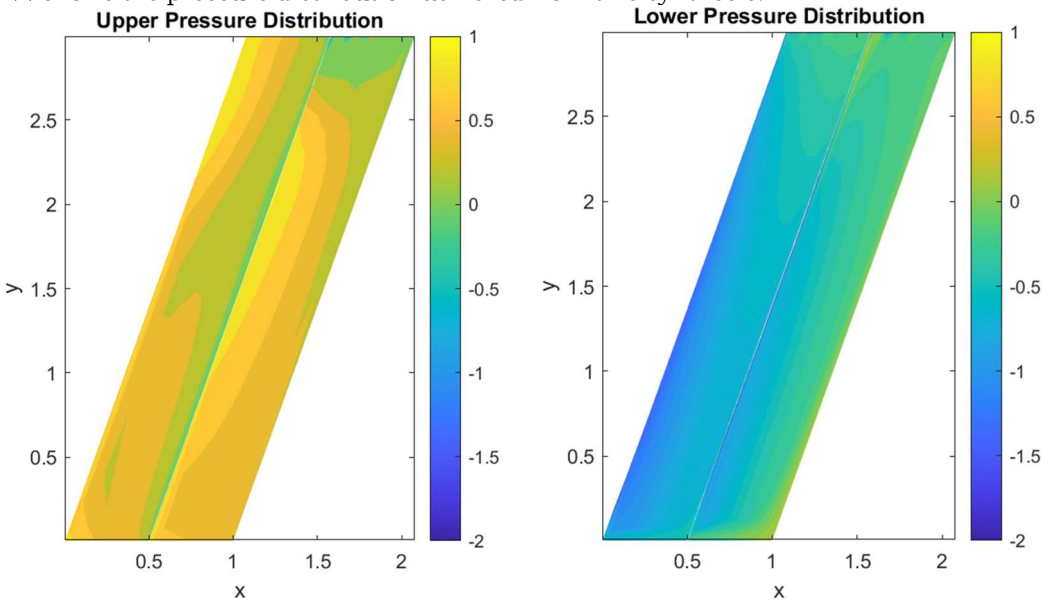

FIGURE 22: Pressure Distribution for Initial 2 Element Wing

The parameters obtained for this portion can be seen in TABLE 3.

TABLE 3: Parameters for 2 Elements of a Multi Element Wing

Control Point	Camber	Front Angle of Incidence in Degrees	Rear Angle of Incidence in Degrees
1	50%	-2.29	-16.70
2	40%	-1.15	-12.95
3	30%	-1.15	-10.20
4	20%	1.15	0.00

Once again, recall that the upper panel is concave, lower panel is convex and the leading edge is pointing downwards during this synthesis as a net downward force is required.

In order to achieve the final synthesis of the wing, we must once again use trial and error and understanding of the perturbation at each point to achieve a satisfactory lift distribution. By making subtle changes at each of the control points on the rear element, the following lift and pressure distributions were obtained.

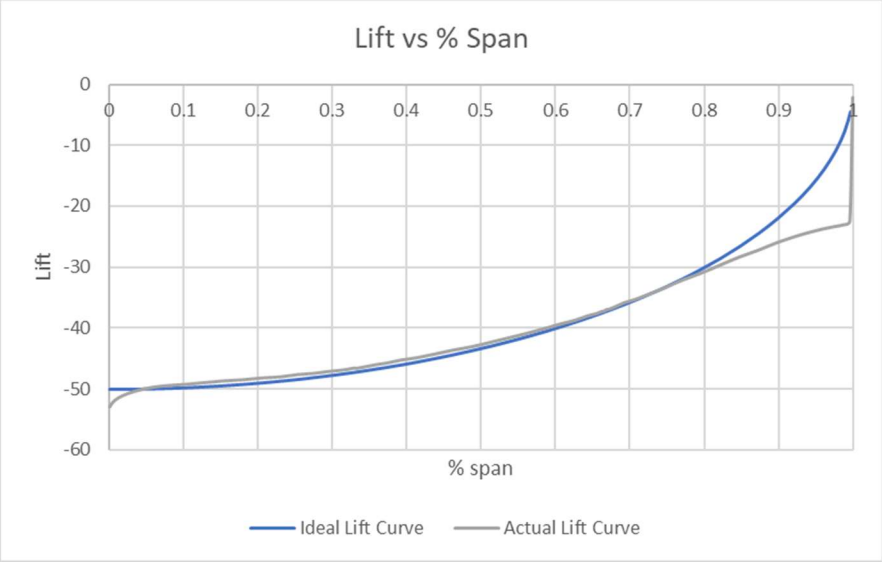

FIGURE 23: Final Synthesized Lift Distribution

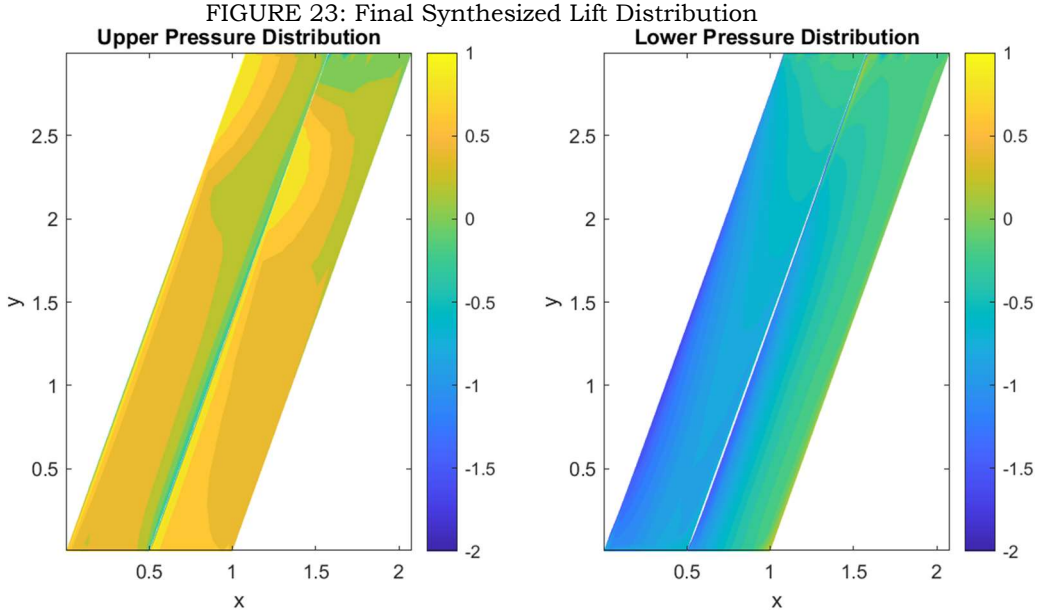

FIGURE 24: Final Synthesized Pressure Distribution

The final parameters obtained for the synthesis of the 2-element wing are shown in TABLE 4, below.

TABLE 4: Parameters for Final Multi Element Wing

Control Point	Camber	Front Angle of Incidence in Degrees	Rear Angle of Incidence in Degrees
1	50%	-2.29	-21.31
2	40%	-1.15	-16.70
3	30%	-1.15	-13.50
4	20%	1.15	0.00

Once again, recall that a net downward force is generated for this synthesis. Therefore, a camber profile with a convex surface on the bottom and a concave surface on top is required and negative angles of incidence are required to point the wing towards the ground.

Similarly, additional wing elements can be synthesized afterwards as needed to add on to the total elements used in the wing design.

D. Alternate Shapes

In order to understand how the different parameters would affect the flow over a multi-element wing, preliminary studies were done before developing a solver algorithm. This provided valuable insight to see how the location of the second wing, the shape of the wing and the overall shape of the wing helps achieve various lift and pressure distributions. This was mostly achieved by changing the planform of the wing. To show a direct and more comparable analysis of this, we will simulate various wing planforms that were tested with identical twist and camber from the one that was synthesized for the 2-element wing. The synthesized parameters were used in this case to show a better comparison of how the lift and pressure distributions vary under the same perturbed camber and twist for each of the control points.

1. Straight Unswept Leading Edge

One of the cases tested was the straight unswept leading edge. Using the following geometry shown in FIGURE 25, the lift and pressure distributions seen in FIGURE 27 and 27 were obtained.

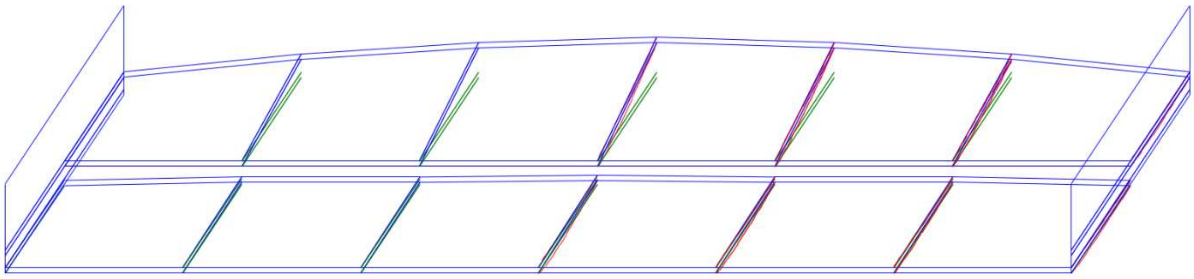

FIGURE 25: Planform of Unswept Wing

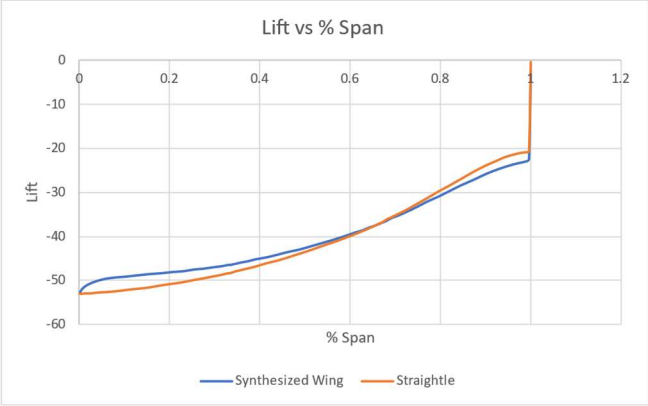

FIGURE 26: Lift Distribution of Unswept Wing

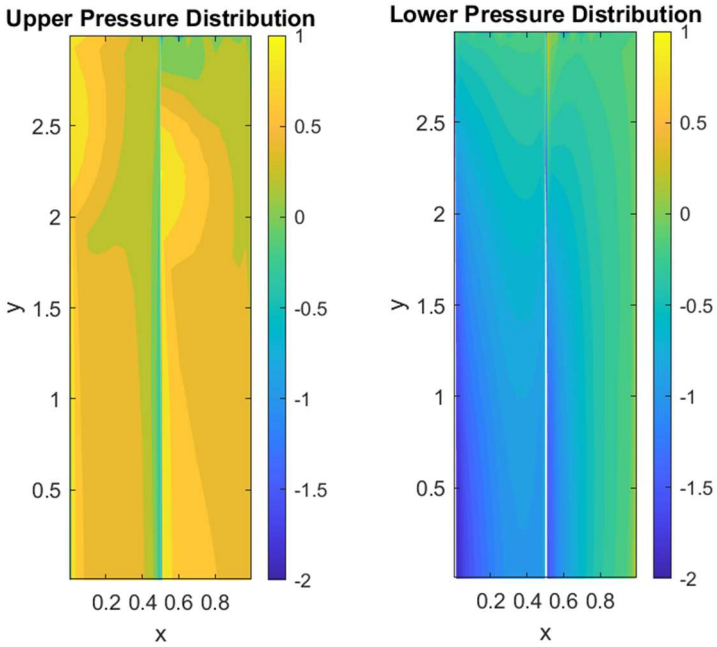

FIGURE 27: Pressure Distribution of Unswept Wing

We see that in the case of the unswept wing with the same lift and camber parameters, the lift generated seems to be comparable to that of the synthesized case with the swept wing. However, it's important to note that the pressures seen at the leading edge of the first element are somewhat higher than expected to be seen.

2. Varying Gap Between Wing Elements

Another parameter that was tested was the gap size and location between wing elements. The location of the 2nd element of the wing was changed to see the changes of airflow over the 2nd element of the wing.

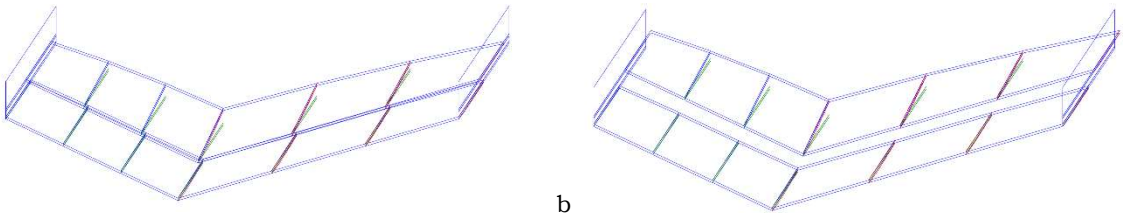
a b
FIGURE 28: Wing Planforms Tested for Gap Effects

a) overlaying wing elements b) increased gap between elements

These gave the lift and pressure distributions seen in FIGURES 28 and 29.

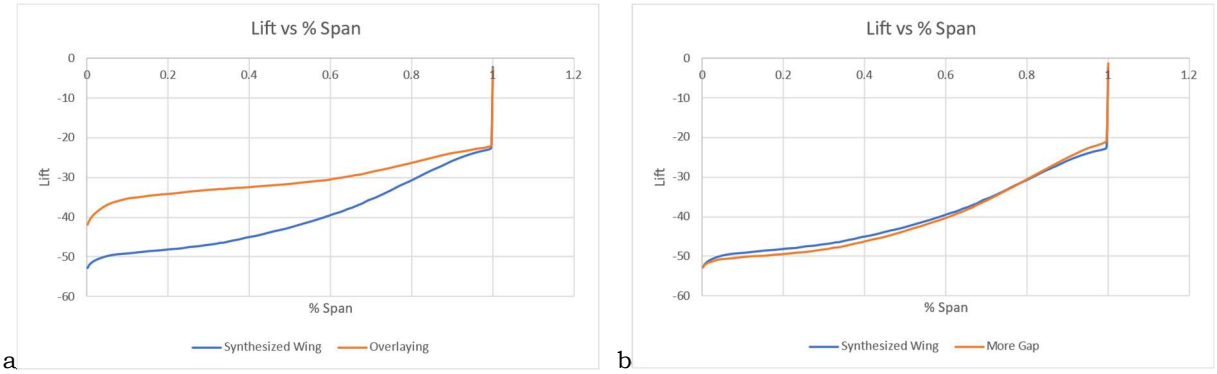

a b

FIGURE 29: Lift Results Obtained by Varying the Gap Between Wing Elements
a) overlaying wing elements b) increased gap between elements

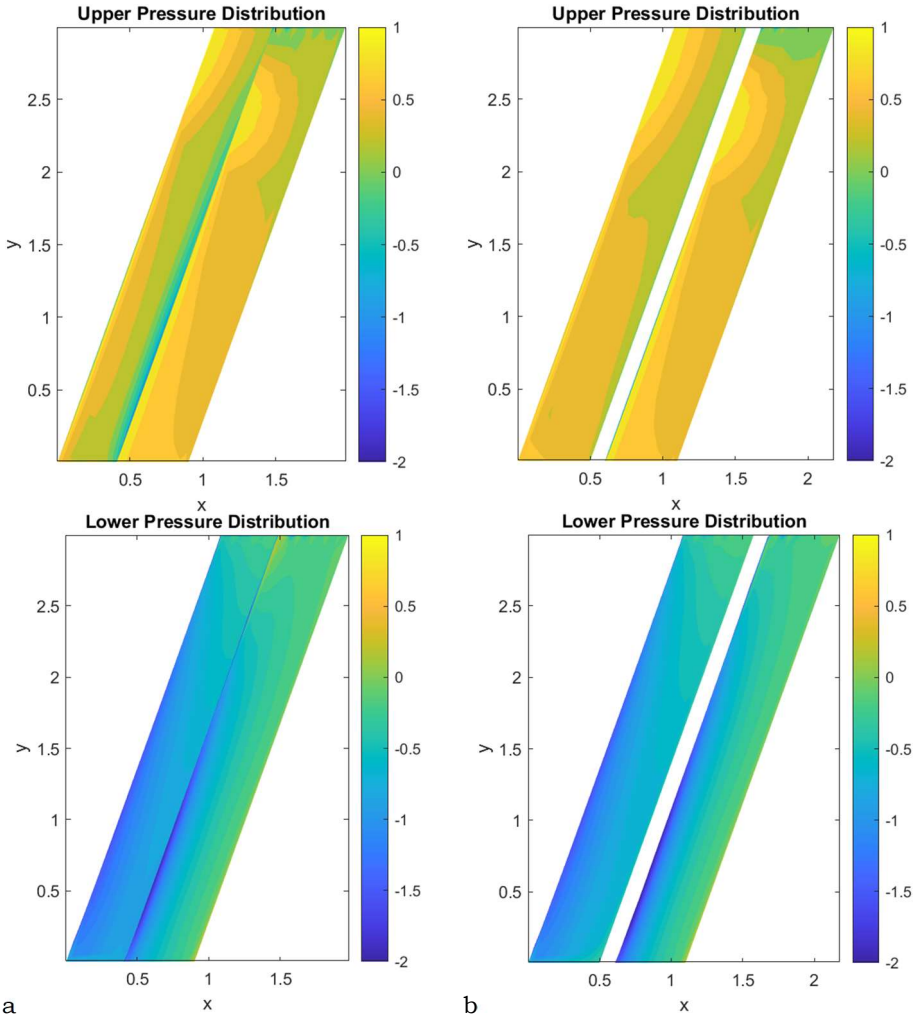

a b

FIGURE 30: Pressure Distributions Obtained by Varying Gap Between Wing Elements
a) overlaying wing elements b) increased gap between elements

We note that in the case with the overlaying wing elements, the lift seems to be less than that of the synthesized wing. This is most likely due to the fact that the area that is overlapped cannot generate as much downforce in the lower (leading) element. For the case with a higher gap between the elements, we note that there is not much variation in the lift curve. We do however note a higher magnitude in the pressures seen on the lower surface of the rear wing element and these are as expected due to the highly twisted element being more open to open wind, as opposed to directed wind from the front element, which results in a higher-pressure gradient occurring on the leading edge.

E. Comparison

TABLE 5 below shows the lift coefficients obtained for the tested wings.

TABLE 5: Lift and Drag Coefficients for Tested Wings

Configuration	CL
Single Element	-0.407
Synthesized Wing	-0.964
Straight LE	-0.994
Overlaying	-0.885
More Gap	-0.980

We see here the difference in performance between each of the modelled wings. The single element wing makes the least lift, CL~0.407. The other wings make substantially more lift, with similar peak suctions. It's also important to note that VORLAX can only compute inviscid drag, so that we will delay any discussion on drag until our next paper where we will use a viscous ANSYS Fluent solution.

VII. Future of Formula 1 Front Wings

During the research conducted, the question was brought up as to what the evolution of front wings for motor racing might hold in the future. As we see motor racing evolve faster than ever before, it is noticeable that more of the downforce generated now comes from the actual body of the racecar and it is clear that this will be the direction that is being followed in the future as well. What this means is that the front wing will most likely mesh with the body of the race car to help with the redirection of flow to critical elements. This would allow the flow to be directed more towards the required portions of the body to generate better flow and also take advantage of the ground effect created by the lower body of the car.

Composite materials also allow Formula 1 cars to maintain the rigidity it needs in the front wing to minimize harm in case of collision but also allow the wing to flex only in certain directions under directional load. What this means is that wings can be manufactured to flex at higher speeds to obtain low drag and then return to high downforce positions under braking as the speeds reduce to get better grip for cornering.

Alternatively, we might also see the return of the split wings seen in FIGURE 4 from the 2015 wings. As the FIA push more and more towards making the field more equal in Formula 1, we have seen less competitive teams being able to take the podium at the end of races in the recent past. In addition, since wind tunnel and simulation times available for teams are more controlled by the FIA [11], the front wings have the potential of becoming more complex and having more complicated structures to redirect airflow to optimize performance.

VIII. Conclusion

Overall, what was noticed in the research conducted was that developing high downforce structures requires a multi-step method to achieve satisfactory results. As the number of elements of a wing increases, there needs to be additional steps taken to achieve the satisfactory lift and pressure distributions in the added elements of the wing.

Another important fact to notice was that we were unable to achieve the lift coefficients of -2.0 using a 2-element wing design. An improvement that could be made to increase this more is to increase the camber utilized in the wing or use a different high lift airfoil entirely. Additionally, increasing the number of elements used in the wing to 4 or 5 elements would also help as the rear elements can then be perturbed at greater angles without flow separation.

However, we can confirm that the move from highly cambered single elements to multi-element wings is feasible for race car applications as it helps create higher downforce while minimizing drag created as well. This also allows higher angles of attack to be applied to the wing elements (especially those that are rearward) to create even more downforce when needed.

In addition, the use of multiple control points in each element of the wing allows for a more resolved wing design with better and improved lift and pressure distributions. This is because each segment of the wing can be modified to obtain the necessary flow over the wing and tweaked until *parc fermé* conditions begin (which prevents teams from working on their cars). Additionally, these also allow for quick tweaks to create downforce in different stints within a race. This is especially useful for different tire uses. For instance, soft tires have a higher grip so a reduced downforce setup can be run on the wing. When switching to a higher compound of tire with lesser grip, the downforce of the wing can be increased to get more grip, so the car doesn't feel significantly different when cornering.

Future work for the research presented in this paper includes testing additional wing elements to understand any additional effects that might be present that were not discovered by using only 2 elements in the presented work. In addition, further simulations will be conducted on ANSYS to verify the results obtained. And finally, a comparison between Formula 1 and Formula E wings might be conducted to understand the different wing designs used in the 2 motorsports.

Appendix

All log files used during the completion of this research can be found at:
https://sajanasr.com/formula-1-wing-design-preliminary-studies/

Please feel free to reach out to the authors for additional documents if required.

Acknowledgments

This manuscript derives from work Mr. Ratnayake performed in partial fulfillment of the degree requirements for obtaining his M.S. in Mechanical Engineering from Arizona State University. All design analysis on this unfunded project was completed at Arizona State University.

References

[1] "1971 - 1972 Ferrari 312 B2 - images, specifications and information," Ultimatecarpage.com Available: https://www.ultimatecarpage.com/car/155/Ferrari-312-B2.html. [Image]

[2] Radu, V., "Ferrari 312T: The forgotten history of formula one's most successful car," autoevolution Available: https://www.autoevolution.com/news/ 23 errari-312t-the-forgotten-history-of-formula-ones-most-successful-car-153121.html. [Image]

[3] "File:Villeneuve's Ferrari 312T4 (paddock).JPG – Wikimedia Commons" Available: https://commons.wikimedia.org/wiki/File:Villeneuve%27s_Ferrari_312T4_(paddock).jpg. [Image]

[4] "Ferrari F1/87," Wikipedia Available: https://en.wikipedia.org/wiki/Ferrari_F1/87. [Image]

[5] "Grand Prix racing history of Scuderia Ferrari," Wikipedia Available: https://en.wikipedia.org/wiki/Grand_Prix_racing_history_of_Scuderia_Ferrari. [Image]

[6] "Ferrari F92A," Wikipedia Available: https://en.wikipedia.org/wiki/Ferrari_F92A. [Image]

[7] "Ferrari 412 T1," Wikipedia Available: https://en.wikipedia.org/wiki/Ferrari_412_T1. [Image]

[8] "Ferrari F2003-GA," Wikipedia Available: https://en.wikipedia.org/wiki/Ferrari_F2003-GA. [Image]

[9] "Ferrari F2005," Wikipedia Available: https://en.wikipedia.org/wiki/Ferrari_F2005. [Image]

[10] “Ferrari SF15-T - new front wing,” *Formula 1® - The Official F1® Website* Available: https://www.formula1.com/en/latest/technical/2015/7/ferrari-sf15-t---new-front-wing.html. [Image]

[11] *2022 FORMULA 1 TECHNICAL REGULATIONS* Available: https://www.fia.com/sites/default/files/2022_formula_1_sporting_regulations_-_iss_5_-_2022-03-15.pdf.

[12] Giuliana, R., “Technical insight: Ferrari with a new front wing in Monza,” *Motorsport Week* Available: https://www.motorsportweek.com/2021/09/13/technical-insight-ferrari-with-a-new-front-wing-in-monza/. [Image]

[13] “How F1 2022's varied front wing designs work,” *The Race* Available: https://the-race.com/formula-1/how-f1-2022s-varied-front-wing-designs-work/. [Image]

[14] How F1 teams combatted porpoising and unleashed performance Available: https://us.motorsport.com/f1/news/f1-teams-porpoising-tech-fix/10322712/ .

[15] Smith, A. M., “High-lift aerodynamics,” *Journal of Aircraft*, vol. 12, 1975, pp. 501–530.

[16] Mayer, J. P., "A Limit Pressure Coefficient and an Estimation of Limit Forces on Airfoils at Supersonic Speeds," Research Memo. L8F23, 1948, NACA.

[17] Seas, “Aerodynamics of F1,” *Technical F1 Dictionary* Available: https://www.formula1-dictionary.net/aerodynamics_of_f1.html.

[18] Küchemann, Dietrich, *The Aerodynamic Design of Aircraft*, AIAA, Virginia, 2012, Chaps. 4, 5.

[19] Stratford, B. S., "The Prediction of Separation of the Turbulent Boundary Layer," *Journal of Fluid Mechanics,* Vol. 5, 1959, pp. 1-16.

[20] Castro, X., and Rana, Z. A., “Aerodynamic and structural design of a 2022 formula One front wing assembly,” *Fluids*, vol. 5, 2020, p. 237.

[21] Ratnayake, S. S., and Takahashi, T. T., “An improved method to synthesize Conceptual Design Wing Lofts,” AIAA SciTech 2021 Forum, 2021.

[22] Ratnayake, S. S., and Takahashi, T. T., “New approaches to direct wing shape synthesis using potential flow solvers,” AIAA SCITECH 2022 Forum, 2022.

[23] Selig, M. S., Guglielmo, J. J., Broeren, A. P., Giguere, P., Williamson, G. A., McGranahan, B. D., Broughton, B. A., Deters, R. W., Brandt, J. B., Lyon, C. A., Gopalarathnam, A., and Ninham, C. P., *Summary of low-speed airfoil data*, Urbana, IL: Department of Aerospace Engineering, University of Illinois at Urbana-Champaign, 1995.

[24] Miranda, L. R., Baker, R. D., and Elliott, W. M., “A Generalized Vortex-Lattice Method for Subsonic and Supersonic Flow,” NASA CR 2875, 1977.

[25] Abbott, I., Von Doenhoff, A. and Stivers, L., “Summary of Airfoil Data,” NACA Report 824, National Advisory Committee for Aeronautics, 1945.